

# Hepatic MDR3 expression impacts lipid homeostasis and susceptibility to inflammatory bile duct obstruction in neonates

Alexandra N. Carey<sup>1,6</sup>, Wujuan Zhang<sup>2,6</sup>, Kenneth D.R. Setchell<sup>2</sup>, Julia R. Simmons<sup>1</sup>, Tiffany Shi<sup>1</sup>, Celine S. Lages<sup>1</sup>, Mary Mullen<sup>1</sup>, Kaitlin Carroll<sup>3</sup>, Rebekah Karns<sup>4</sup>, Kazuhiko Bessho<sup>1</sup>, Rachel Sheridan<sup>2</sup>, Xueheng Zhao<sup>2</sup>, Susanne N. Weber<sup>5</sup> and Alexander G. Miethke<sup>1</sup>

**BACKGROUND:** Heterozygous mutations in the gene *ABCB4*, encoding the phospholipid floppase MDR3 (*Mdr2* in mice), are associated with various chronic liver diseases. Here we hypothesize that reduced *ABCB4* expression predisposes to extrahepatic biliary atresia (EHBA).

**METHODS:** Livers from neonatal wild-type (wt) and heterozygous *Mdr2*-deficient mice were subjected to mass spectrometry-based lipidomics and RNA sequencing studies. Following postnatal infection with rhesus rotavirus (RRV), liver immune responses and EHBA phenotype were assessed. Hepatic microarray data from 40 infants with EHBA were mined for expression levels of *ABCB4*.

**RESULTS:** Phosphatidylcholine (PC) and phosphatidylethanolamine (PE) were increased, whereas the PC/PE ratio was decreased in neonatal *Mdr2*<sup>+/-</sup> mice compared with wt mice. Following RRV challenge, hepatic expression of IFN $\gamma$  and infiltration with CD8+ and NK+ lymphocytes were increased in *Mdr2*<sup>+/-</sup> mice. Plasma total bilirubin levels and prevalence of complete ductal obstruction were higher in these mice. In infants with EHBA, hepatic gene expression of *ABCB4* was downregulated in those with an inflammatory compared with a fibrosing molecular phenotype.

**CONCLUSION:** Decreased expression of *ABCB4* causes dysregulation in (phospho)lipid homeostasis, and predisposes to aberrant pro-inflammatory lymphocyte responses and an aggravated phenotype of EHBA in neonatal mice. Downregulated *ABCB4* is associated with an inflammatory transcriptome signature in infants with EHBA.

The main constituents of bile, including bile acids (BA), phospholipids (PL; mainly phosphatidylcholines), and cholesterol, are actively excreted from hepatocytes into the bile across the canalicular membrane by the proteins BSEP (encoded by the gene *ABCB11*), MDR3 (*ABCB4*), and ABCG5/8 (*ABCG5/8*), respectively, all of which are members of the ABC transporter family. Impaired expression of these

transporters results in well-recognized clinical syndromes of chronic cholestasis, typically with onset in infancy. The most severe phenotypes result from biallelic mutations in the respective genes—for instance, in progressive familial intrahepatic cholestasis (PFIC) type 2 due to mutations in *ABCB11*, a syndrome of chronic cholestasis associated with low or normal serum gamma-glutamyltransferase activity and absent or low levels of bile salts in bile—whereas dual mutations in *ABCB4* cause a fibrosing cholangiopathy with high serum gamma-glutamyltransferase levels and absence of biliary PL. MDR3 disease is associated with a variety of liver disease phenotypes, ranging from neonatal onset of cholestatic jaundice, commonly referred to as PFIC type 3, to low phospholipid intrahepatic gallstones and biliary fibrosis with characteristic radiographic and histologic features (1–3). Histologically it is characterized by a cholangiopathy with bile duct epithelial injury and ductal proliferation, portal inflammation, and variable stage of fibrosis. Deficiency of MDR3 in humans, or of the ortholog *Mdr2* in mice, was shown to reduce biliary PL concentration and to predispose to biliary microcrystal formation, cholangiocyte injury, and hepatocellular carcinoma (4).

A recent population-based genome sequencing study in Iceland detected four variants in the gene *ABCB4* that confer risk for the development of gallstones, intrahepatic cholestasis of pregnancy (ICP), HCC and cholangiocarcinoma, and cirrhosis (5), thus rendering *ABCB4* the gene with perhaps the most significant contributions to inherited liver disease, similar to that of the *PNPLA3*. Importantly, there has been increasing evidence for rare *ABCB4* variants causing liver disease in both autosomal dominant and recessive inheritance patterns. For instance, heterozygous missense mutations, which impair trafficking of MDR3, were associated with ICP (6). Heterozygous mutations in *ABCB4* have also been linked to idiopathic fibrosing cholestatic liver disease in adults (7), chronic cholestatic biochemistry profile and family history of liver disease (8), and early onset of primary sclerosing cholangitis (8). Recently, heterozygous variants in

<sup>1</sup>Division of Pediatric Gastroenterology, Hepatology, and Nutrition, Cincinnati Children's Hospital Medical Center (CCHMC), Cincinnati, Ohio; <sup>2</sup>Division of Pathology and Laboratory Medicine, CCHMC, Cincinnati, Ohio; <sup>3</sup>Division of Immunobiology, CCHMC, Ohio; <sup>4</sup>Division of Biomedical Informatics, CCHMC, Ohio; <sup>5</sup>Klinik fuer Innere Medizin II, Universitaetsklinikum des Saarlands, Homburg, Germany. Correspondence: Alexander G. Miethke (alexander.miethke@cchmc.org)

<sup>6</sup>The first two authors contributed equally to this work.

Received 19 July 2016; accepted 6 March 2017; advance online publication 3 May 2017. doi: 10.1038/pr.2017.78

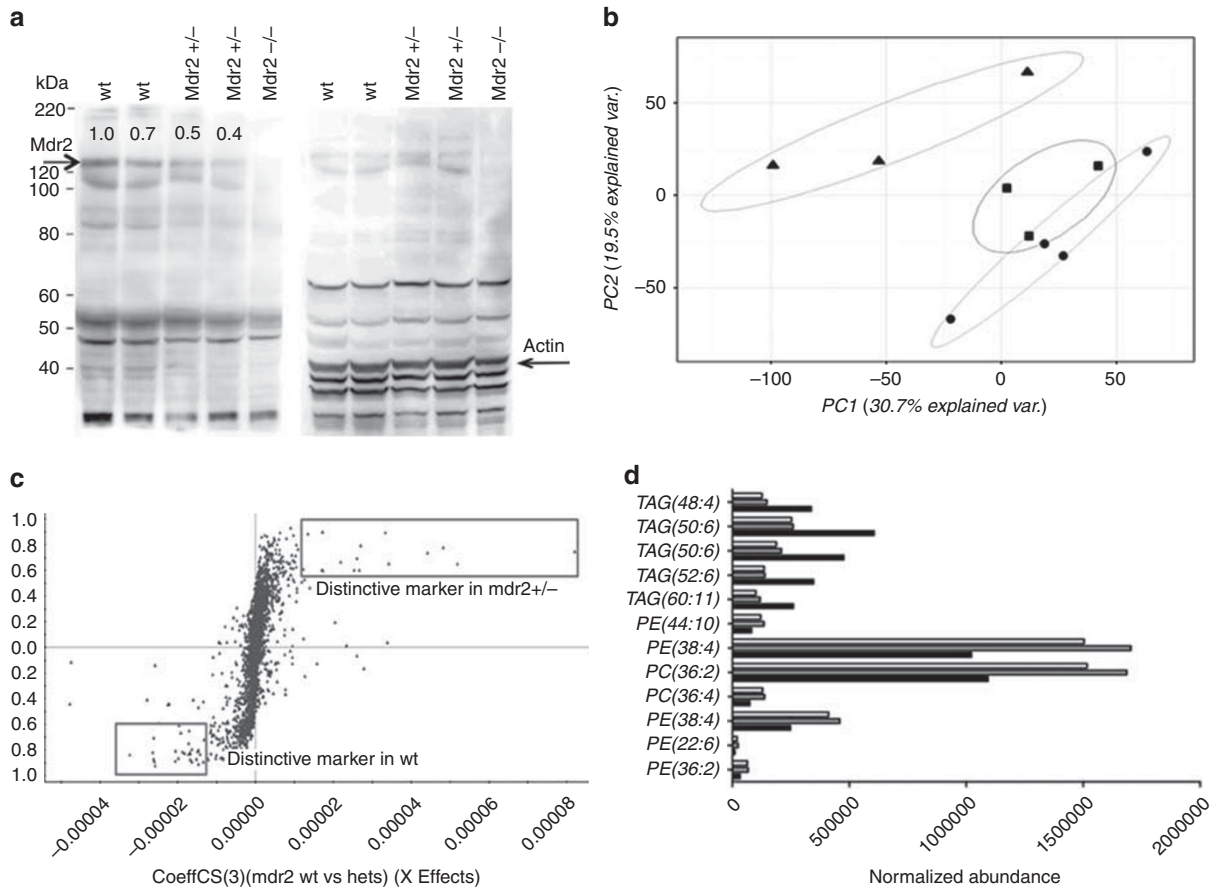


**Figure 1.** Liver lipidomic patterns distinctly differ between neonatal wild-type (wt) and *Mdr2*<sup>+/-</sup> mice. Protein blot analysis of crude hepatic protein extracts from neonatal mice was performed by sodium dodecyl sulfate-polyacrylamide gel electrophoresis. Numbers on the blot in the left panel denote relative densitometry values for the intensity of the *Mdr2* band at 140 kDa normalized against the specific band recognized by the anti-actin antibody at 43 kDa in the right panel (a). Principal component analysis (PCA) of a total of 7,281 features (4,502 negative compound ions and 2,779 positive compound ions) detected by mass spectrometry (MS) on liver tissue homogenates from neonatal *Mdr2*<sup>-/-</sup> mice (denoted as circles), *Mdr2*<sup>+/-</sup> (squares), and wt mice (triangles) following exhaustive lipid extraction; MS analysis was performed in triplicate for each sample and the intensity of each compound ion is reported as average of three injections (b). S-plot comparing *Mdr2*<sup>+/-</sup> (right upper quadrant) with wt (left lower quadrant), with each point representing one of the 2,779 positive compound ions. Compounds farthest away from Y axis correspond to significantly changed metabolites in each group (c). Quantification of lipid species from metabolomic analysis shows that phosphatidylcholines (PCs) and phosphatidylethanolamines (PEs) accumulate, whereas several triglyceride (TAG) species are reduced in livers of *Mdr2*<sup>+/-</sup> (gray-fill columns) and *Mdr2*<sup>-/-</sup> (no-fill columns) compared with wt mice (black-fill columns) in (d).

*ABCB4* were also detected in a cohort of nine children with idiopathic chronic cholestasis with first onset of symptoms between 2 months and 11 years of age (9). In five subjects, haploinsufficiency for *ABCB4* was associated with other liver diseases, including extrahepatic biliary atresia (EHBA). Coexistence of heterozygous variants in *ABCB4* and in functionally related genes such as *ABCB11* and *ATP8B1* was found to be more frequent in children with idiopathic cholestasis than in healthy controls (10). However, the mechanisms by which reduction in MDR3 expression due to heterozygous mutations modulates coexisting liver diseases are currently unknown.

**RESULTS**

Reduced expression of the protein *Mdr2* in neonatal *Mdr2*<sup>+/-</sup> compared with wild-type (wt) mice was confirmed by immunoblotting (Figure 1a). In order to characterize the

influence of *Mdr2* expression on the hepatic microenvironment in neonatal mice, we performed global lipidomic studies on liver samples. Principal component analysis of a total of 7,281 combined positive and negative compound ions acquired by accurate mass measurement revealed that *Mdr2*<sup>+/-</sup> mice clustered more closely in their metabolic signature with homozygous knockout and both genotypes were largely segregated from wt mice (Figure 1b). Compounds that significantly accumulated in the liver of *Mdr2*<sup>+/-</sup> mice included several phosphatidylcholine (PC) and phosphatidylethanolamine (PE) species—i.e., PC (36:4), PC(36:2), PE (36:4), and PE (44:10)—with their identity confirmed either with available reference standards or using our in-house lipid database. Meanwhile, the hepatic levels of several triglyceride (TAG) species, including TAG (48:4) and TAG (60:12), were decreased in *Mdr2*<sup>+/-</sup> compared with wt mice (Figure 1c,d).

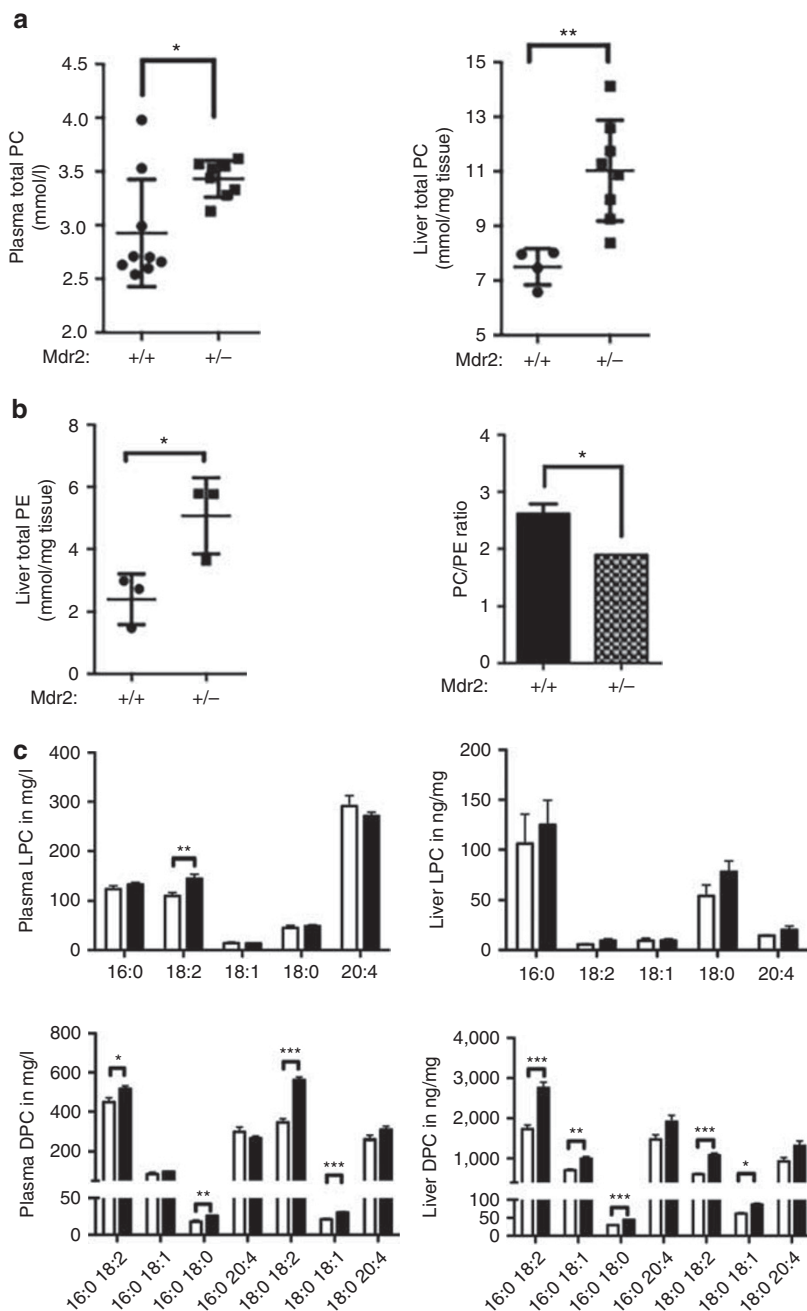


**Figure 2.** Neonatal *Mdr2*<sup>+/-</sup> mice accumulate total and individual phosphatidylcholine (PC) and phosphatidylethanolamine (PE) species. Phospholipids were extracted from liver homogenates and plasma of 10-day-old mice of *Mdr2*<sup>+/-</sup> and wt mice, and subjected to targeted mass spectrometry to measure the concentrations of PC (a), of PE (b), and of individual lyso- and diacylphosphatidylcholines (LPC/DPC) (c). Black-filled columns denote *Mdr2*<sup>+/-</sup> mice (n=8) and no-fill columns denote wt mice (n=9). Unpaired t-test was applied to test for statistically significant differences between groups with \*P<0.05, \*\*P<0.01, and \*\*\*P<0.005. Each dot in (a and b) represents a value from an individual animal.

Candidates from this global lipidomics analysis were confirmed by targeted mass spectrometry-based quantitative analysis of PLs, which revealed that total PC concentration was significantly higher in liver and plasma in neonatal *Mdr2*<sup>+/-</sup> compared with wt mice (Figure 2a). The other predominant hepatic phospholipid class, PE, was also found to accumulate in *Mdr2*<sup>+/-</sup> mice compared with wt mice.

Targeted quantitative analysis of both PC and PE validated the lipid data acquired in an unbiased manner on the quadrupole time-of-flight mass spectrometry platform (Figure 2b). Importantly, the ratio of PC/PE, which was previously shown to negatively correlate with liver injury and impaired regeneration (11), was decreased in *Mdr2*<sup>+/-</sup> compared with wt mice (molar ratio of PC/PE: 2.6 vs. 1.9

in neonatal wt vs. *Mdr2*<sup>+/-</sup>, *P*<0.05). For individual PL species, we found the concentrations for 18:2 lysophosphatidylcholines (LPCs), and several diacyl phosphatidylcholines to be significantly increased in plasma and liver of neonatal *Mdr2*<sup>+/-</sup> mice (Figure 2c).

To further characterize the effects of reduced *Mdr2* expression on liver metabolic and immune function in these mice, we performed RNA sequencing (RNAseq). Genes associated with cholesterol and lipid metabolism were primarily downregulated in neonatal *Mdr2*<sup>+/-</sup> mice, including expression of the phosphatidylcholine transfer protein *pctp* gene, which may contribute to retention of PLs in livers from *Mdr2*<sup>+/-</sup> mice (Figure 3a,b). Interestingly, genes associated with immune function were also differentially regulated in *Mdr2*<sup>+/-</sup> compared with wt mice. For instance, genes involved in T-lymphocyte polarization, such as *irf4* and *il12a*, were upregulated in *Mdr2*<sup>+/-</sup> mice, whereas hepatic mRNA for genes linked to co-stimulation control of T-lymphocytes, such as *icos* and *cd27*, was reduced (Figure 3c). These findings of MS-based global lipidomic and RNAseq studies raise the biological possibility that diminished hepatic expression of *mdr2* renders the hepatic microenvironment to amplify pro-inflammatory responses upon challenge with appropriate triggers.

To test this hypothesis, we challenged neonatal *Mdr2*<sup>+/-</sup> and wt mice with an attenuated dose of RRV. By day 8 post RRV (p RRV), the virus was not actively replicating in the livers from mice of both genotypes, as shown by quantitative PCR (qPCR) for the RRV-specific viral protein VP6 (Figure 4a) and for NSP3 (data not shown). In the conventional model of RRV-induced EHBA using a higher virus dose, hepatic expression of these viral proteins peaks at day 7 p RRV and rapidly disappears thereafter (12). Following RRV infection, *Mdr2* mRNA expression was upregulated in wt and *Mdr2*<sup>+/-</sup> mice (Figure 4b). Flow cytometry, revealed increased infiltration of the liver with NK and CD8 lymphocytes in *Mdr2*<sup>+/-</sup> compared with wt littermates on day 8 p RRV (Figure 4c). Using multiplex gene expression profiling, we found upregulation (≥2-fold) of 16 pro-inflammatory genes including *cxcl-10* and *-11*, inducible nitric oxide synthase (*inos*), and *sele*, encoding E-selectin, in RRV-infected *Mdr2*<sup>+/-</sup> compared with wt mice (Figure 4d). Candidate gene expression studies with SYBR green qPCR confirmed upregulation of the Th1 and Th2 cytokines interferon-gamma (*ifny*) and interleukin (*il5*), respectively (Figure 4e). Both cytokines were previously recognized to be key drivers of neonatal bile duct obstruction (12,13). The upregulation of *inos* in *Mdr2*<sup>+/-</sup> mice, whose role in murine EHBA is largely undefined, was corroborated by immunohistochemical studies showing increased immunoreactivity against iNOS in inflammatory cells infiltrating the portal triads of livers from RRV-infected *Mdr2*<sup>+/-</sup> mice (Figure 4f).

In order to ascertain whether aggravated hepatic inflammation and immune activation in RRV-infected *Mdr2*<sup>+/-</sup> mice influenced their EHBA phenotype, we determined plasma levels for total bilirubin, a circulating biomarker for biliary

obstruction, and ductal patency by histomorphological analysis. Total bilirubin levels were significantly increased in RRV-infected *Mdr2*<sup>+/-</sup> compared with wt littermates (Figure 5a). Furthermore, complete inflammatory obstruction of the bile ducts was fourfold more common in animals with heterozygous loss of *mdr2* compared with controls (Figure 5b).

To validate our findings in human samples, we surveyed the patients at our institution with the clinical diagnosis of MDR3 disease and found one subject with dual diagnosis of MDR3 disease and EHBA. The liver explant of this 23-month-old girl was remarkable for biliary cirrhosis (Figure 6aA). In addition to changes typically seen in EHBA, for instance, absent gallbladder, complete obliteration of the extrahepatic bile ducts (Figure 6aB), and bile duct proliferation with bile plugs (Figure 6aD), features of MDR3 disease were also present, including intrahepatic gallstones (Figure 6aC) and canalicular cholestasis (Figure 6aE). This observation raised the possibility that in humans, similar to mice, reduced expression of the phospholipid floppase MDR3 predisposed to inflammatory hepatobiliary injury in the neonate. In order to further interrogate this hypothesis, we mined previously generated hepatic gene expression data from a cohort of 40 infants with EHBA (14). On the basis of the liver transcriptome, 36 subjects were assigned either an inflammatory (*n*=14) or a fibrosing molecular phenotype (*n*=22), using previously reported bioinformatics algorithms (15). In this cohort, mRNA expression for *ABCB4* was significantly lower in 14 subjects with an inflammatory phenotype, characterized by upregulation of genes linked to the activation of the pro-inflammatory transcription factors *NFKB* and *NFAT*, compared with the group with a fibrosing molecular phenotype, in which genes that encode proteins with binding sites for the profibrogenic transcription factors *E2F* and *SP1* were abundantly expressed (Figure 6b).

## DISCUSSION

We have demonstrated that heterozygous loss of *Mdr2* in neonatal mice leads to alterations in the hepatic and plasma lipid profiles, differential expression of genes involved in lipid metabolism and immune function, and predisposes to pro-inflammatory and enhanced polarized lymphocyte responses in the liver upon postnatal challenge with RRV. *Mdr2*<sup>+/-</sup> mice display an aggravated obstructive phenotype of EHBA compared with wt mice. In humans, decreased hepatic expression of *ABCB4* is associated with a molecular signature of inflammatory EHBA. Collectively, our data suggest that genetically determined alterations in hepatic PL metabolism may modulate hepatic immune function and confer susceptibility to inflammatory hepatobiliary injury in the neonate.

Systematic analysis of liver and plasma lipid and PL concentrations has not been performed in neonatal *Mdr2*<sup>+/-</sup> mice before. Previous studies in adult wt and *Mdr2*<sup>-/-</sup> mice demonstrated decreased concentration of serum PL in the knockout mice (16). Contrary to the findings in adult mice,

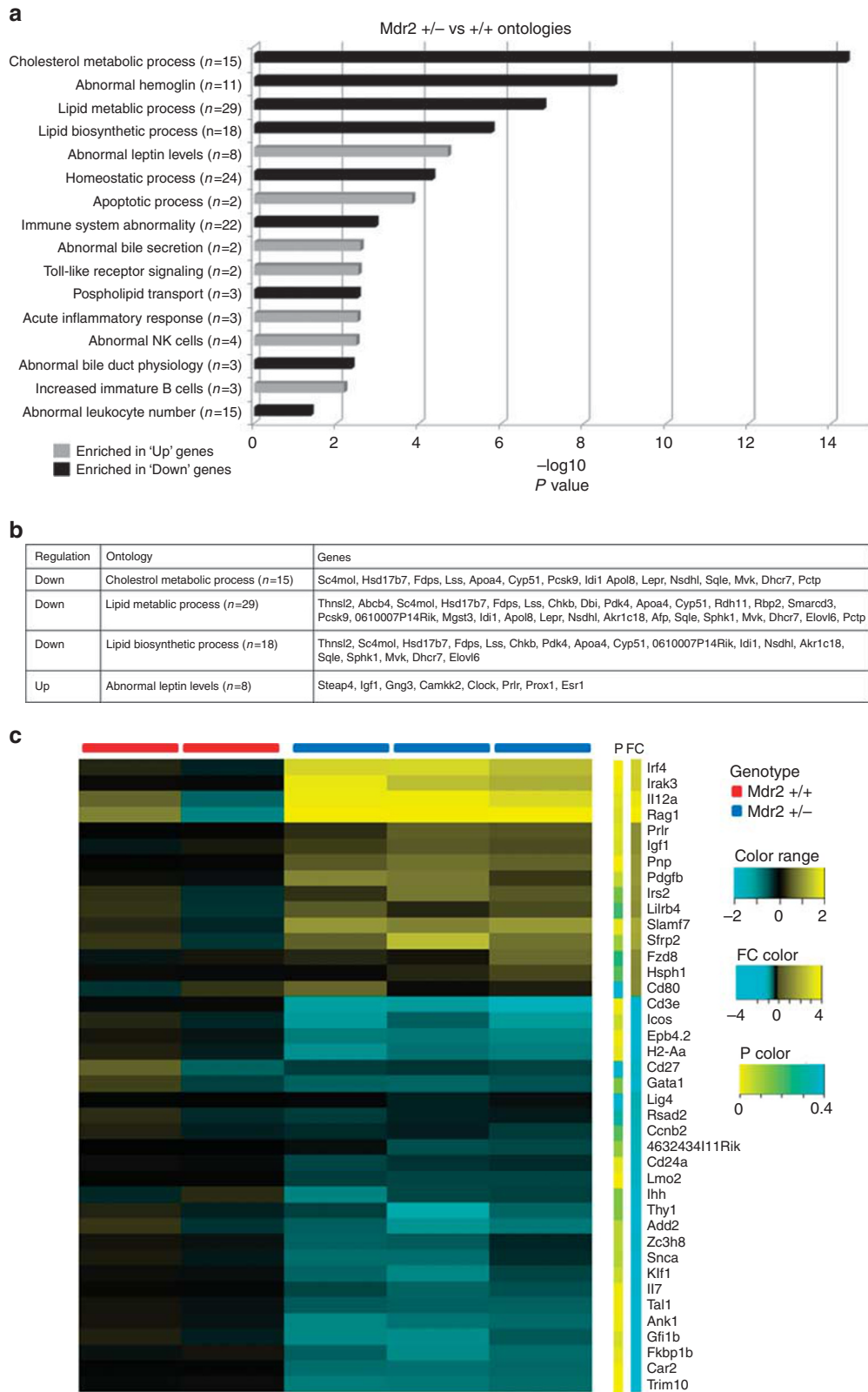


**Figure 3.** Global transcriptomic profiles in livers of neonatal *Mdr2*<sup>+/-</sup> and wt mice. RNAseq studies were performed on total hepatic RNA from 10-day-old *Mdr2*<sup>+/-</sup> and *Mdr2*<sup>+/+</sup> mice. On the basis of the pathway enrichment analysis, 16 pathways comprising significantly upregulated or downregulated genes in *Mdr2*<sup>+/-</sup> compared with *Mdr2*<sup>+/+</sup> control mice are depicted, with *P* values for these pathways plotted as  $-\log_{10}$  (a). Differentially expressed genes regulating lipid metabolisms are listed in (b). Forty genes from pathways relevant for immune function are displayed in the heatmap with expression levels normalized to control *Mdr2*<sup>+/+</sup> mice (c).

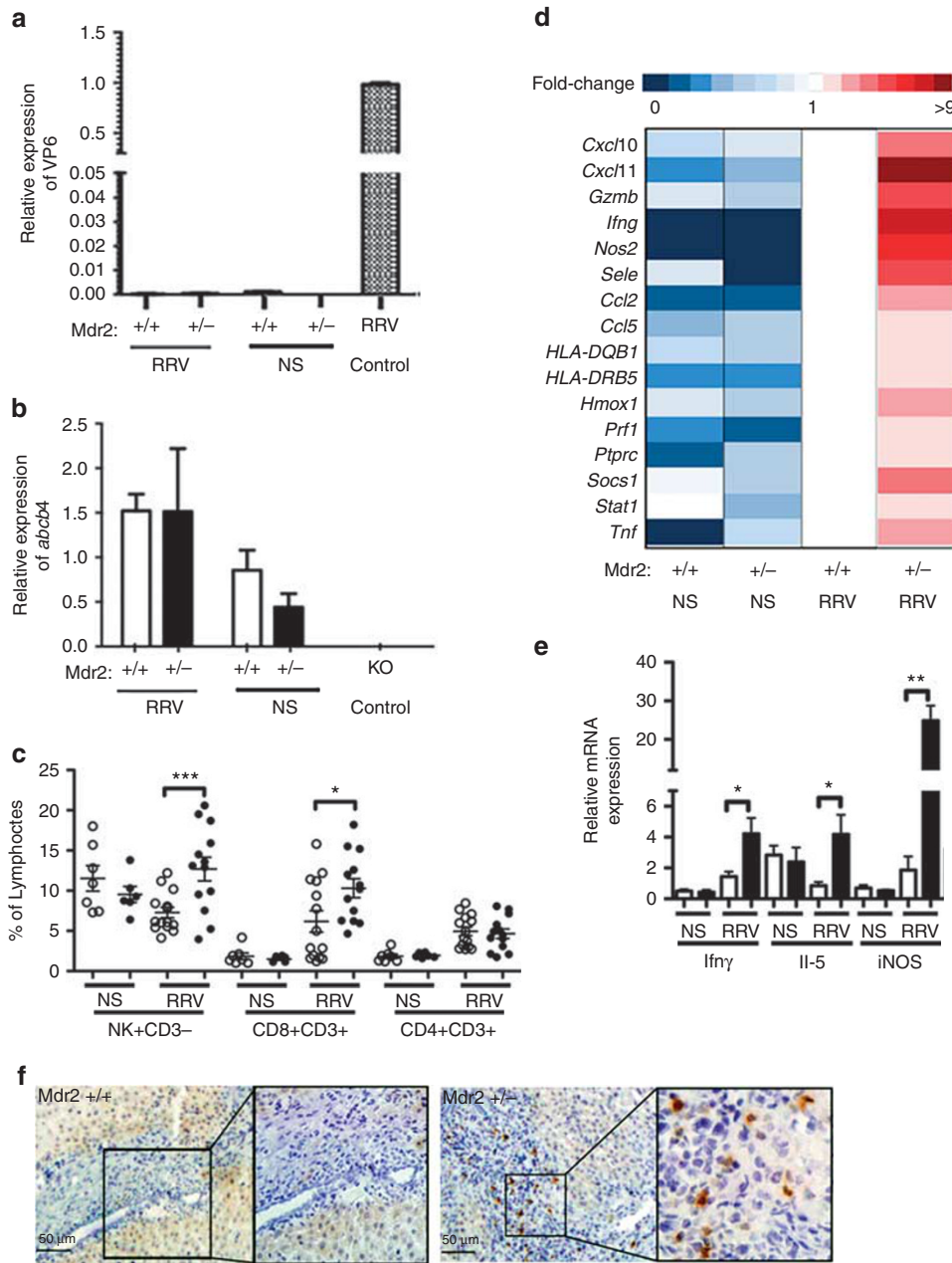


**Figure 4.** Hepatic pro-inflammatory gene expression and effector lymphocyte recruitment following postnatal viral challenge of wt and *Mdr2*<sup>+/-</sup> mice. Livers were harvested on day of life 10 following postnatal administration of rhesus rotavirus (RRV) or normal saline (NS). Hepatic expression of RRV-specific VP6 in *Mdr2*<sup>+/-</sup> and *Mdr2*<sup>+/+</sup> mice (n = 3 per group) was quantified by SYBR green quantitative PCR (qPCR) and was compared with the expression levels in infected cholangiocytes serving as positive control (a). Regulation of *Abcb4* mRNA expression following RRV infection was determined by TaqMan qPCR, with hepatic mRNA from an *Mdr2*<sup>-/-</sup> mouse serving as negative control (b). Hepatic mononuclear cells were subjected to flow cytometry, and specific lymphocyte frequencies were determined within the size-gated lymphocyte population. Every dot represents % lymphocytes in an individual animal. No-fill circles denote wt, black-filled circles denote *Mdr2*<sup>+/-</sup> mice (c). Multiplex qPCR for 88 cytokines and chemokines was performed using TaqMan Mouse Immune Arrays. The heatmap shows genes with >2-fold upregulation in RRV-infected *Mdr2*<sup>+/-</sup> vs. wt mice (d). Candidate gene expression studies on hepatic RNA were performed using SYBR green qPCR. No-fill columns denote wt, black-filled columns represent *Mdr2*<sup>+/-</sup> mice with n = 6 animals per group (e). Protein expression of iNOS was detected by immunohistochemistry (f). Unpaired t-test was applied to test for statistical differences between groups in (c and e), with \*P < 0.05, \*\*P < 0.01, and \*\*\*P < 0.005.

we found increased hepatic concentrations of PC and PE and lower levels of TAG in the neonatal *Mdr2*<sup>+/-</sup> and *Mdr2*<sup>-/-</sup> mice compared with wt animals.

The lipidomic profile of neonatal *Mdr2*<sup>+/-</sup> resembles more closely that of *Mdr2*<sup>-/-</sup> mice than wt mice. The reasons for

this observation are unknown. We can only speculate that “physiologic cholestasis”, caused by the immaturity of the neonatal liver in terms of bile acid and organic anion transporter development (17) and specifically the expression of *Mdr2* transcripts (18), further reduces *Mdr2*-mediated

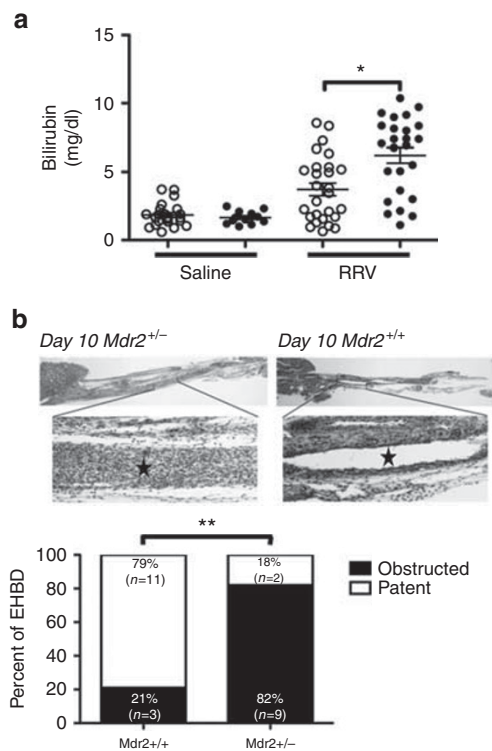


**Figure 5.** Reduced *Mdr2* expression predisposes to extrahepatic bile duct obstruction following rhesus rotavirus (RRV) challenge. Total bilirubin concentrations were measured by colorimetric analysis in plasma samples obtained from neonatal *Mdr2*<sup>+/+</sup> (denoted by no-fill circles) and *Mdr2*<sup>+/-</sup> mice (black-filled circles) 8 days after injection of either low-dose RRV or normal saline intraperitoneally on day of life 2 (a). Bile ducts were microdissected on day 8 p RRV, and hematoxylin and eosin-stained longitudinal consecutive sections were examined for patency or obstruction. Representative photomicrographs from bile ducts of both groups of mice with \* denoting the bile duct lumen are shown in (b). Unpaired t- and Fisher exact tests were applied to test for statistical differences between groups in (a and b), respectively, with \**P* < 0.05, \*\**P* < 0.01.

phospholipid floppase activity in neonates, rendering the lipidomic profile in these mice more similar to homozygous knockout mice. The reduction of TAG in neonatal *Mdr2*<sup>+/-</sup> mice is noteworthy, as loss in TAG storage capacity is critically linked to lipotoxicity and has been shown to exacerbate liver injury (19). Aiming at this metabolic pathway, high-fat diet has been reported to increase hepatic TAG levels and to reverse liver injury in *Mdr2*<sup>-/-</sup> mice. Maternal intake of this diet was sufficient to inhibit the development of sclerosing cholangitis and fibrosis in *Mdr2*<sup>-/-</sup> offspring (16).

Targeted quantitative analysis of liver tissue revealed increased total concentrations of PC and PE, and a decrease in the hepatic PC/PE ratio. These two classes of phospholipids are asymmetrically distributed in the plasma membrane: PCs are mainly on the outer leaflet and PEs are preferentially located on the inner leaflet, which makes the PC/PE ratio critical for plasma membrane permeability (20). Hepatic PC homeostasis is regulated by several processes, including biosynthesis from PE through the PE *N*-methyltransferase

(PEMT) pathway and efflux into the bile facilitated by *Mdr2*. Mice deficient in *Pemt* develop steatohepatitis and acute liver failure within 3 days of starting a choline-deficient diet (21), which is linked to a reduced PC/PE ratio and impaired membrane integrity. When this ratio is increased, liver injury can be prevented (11). Hepatic PC/PE has also been reported to be inversely correlated with the development of steatosis and inflammation in the progression of NAFLD (22). Consistent with the literature on disease progression in inflammatory liver diseases, our lipidomic data suggest that a decreased PC/PE ratio in *Mdr2*<sup>+/-</sup> mice may render these animals more susceptible to hepatobiliary injury during the neonatal period. To what degree our findings on lipid homeostasis in neonatal *Mdr2*<sup>+/-</sup> and *Mdr2*<sup>-/-</sup> mice in BALB/c background can be generalized to mice with impaired phospholipid floppase activity in other background strains requires further investigations. Progression of sclerosing cholangitis is reported to be accelerated in *Mdr2*<sup>-/-</sup> mice of BALB/c compared with FVB and C57BL6 backgrounds (23). Whether strain-specific differences in cholesterol and phospholipid absorption and lipoprotein formation, for which the FVB strain is known to be a high HDL producer conferring resistance to atherosclerosis (24), also influence the liver disease phenotype is unknown. Strain-specific differences for kinetics of serum biochemistries correlating with cholestasis in *Mdr2*<sup>-/-</sup> mice were recently reported (25,26).

We also found increased plasma concentrations for individual LPC and diacylphosphatidylcholines species. LPCs have previously been linked to the control of inflammatory pathways, especially during sepsis (27). Furthermore, LPC is known to induce IFN $\gamma$  production by CD4+ lymphocytes (28), linking local tissue regulation of LPC and T-cell activation with inflammatory tissue destruction, for instance in atherosclerosis. Additional help to T-cell activation may be derived from LPC-associated maturation of professional antigen-presenting cells and control of Toll-like receptors on monocytes (29). In our experimental setting, increased plasma and liver LPC/diacylphosphatidylcholines concentrations in neonatal (noninfected) *Mdr2*<sup>+/-</sup> mice were associated with the upregulation of hepatic expression of *Il12a* and *Irf4*, encoding proteins polarizing naive T lymphocytes to a Th1 or Th2 phenotype, respectively. Following low-dose RRV challenge, hepatic gene expression for *Ifny* and *Il5* was higher in *Mdr2*<sup>+/-</sup> compared with infected wt mice. Both cytokine pathways have previously been linked to ductal obstruction in EHBA (30). Surges in the expression of pro-inflammatory cytokines in *Mdr2*<sup>+/-</sup> mice correlated with liver infiltration with NK and CD8 lymphocyte responses, both found to be effector lymphocytes of neonatal bile duct obstruction (31,32), and an aggravated EHBA phenotype. Several details on how the metabolic hepatic microenvironment predisposes to accelerated hepatobiliary injury in neonatal *Mdr2*<sup>+/-</sup> mice remain unknown. Although our experiments demonstrate that mRNA and protein expressions for *mdr2* are both significantly reduced in neonatal, noninfected *Mdr2*<sup>+/-</sup> mice compared with wt mice, RRV infection causes upregulation of

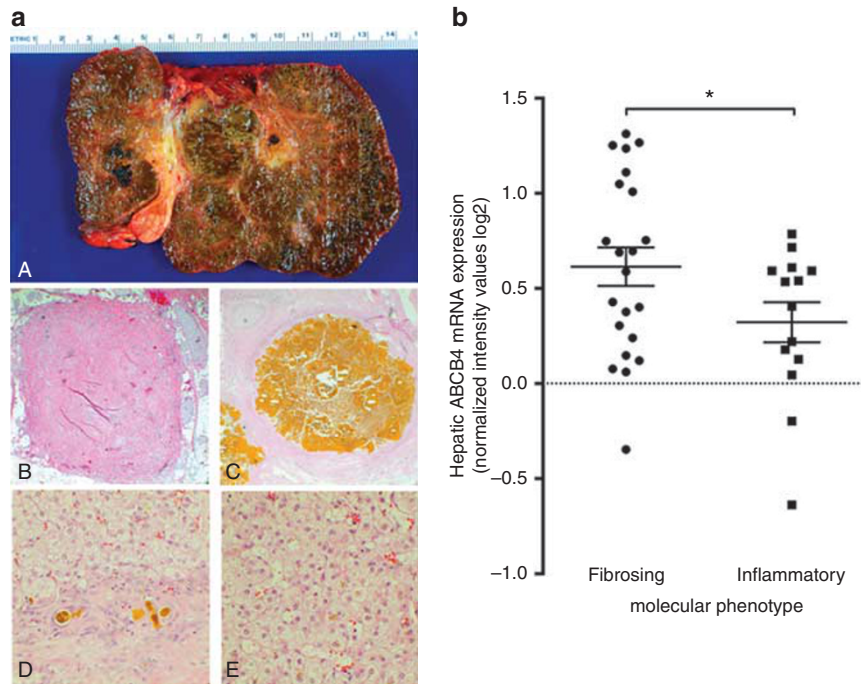


**Figure 6.** Association between hepatic expression of *ABCB4* mRNA and inflammatory molecular signature in infants with extrahepatic biliary atresia (EHBA). (aA) Explanted liver of a 23-month-old Somali girl with the clinical diagnosis of MDR3 disease, supported by biallelic nonsynonymous variants in *ABCB4*. The explant shows biliary cirrhosis and (aB) complete fibrous obliteration of the extrahepatic bile duct, (aD) bile duct proliferation with bile plugs, (aC) intrahepatic gallstones, and (aE) canalicular cholestasis. Decreased hepatic expression of *ABCB4* in subjects with a transcriptomic profile of inflammatory EHBA is shown in (b). Hepatic microarray gene expression data from a study on 40 subjects with EHBA identifying molecular signatures for inflammatory and fibrosing phenotypes were mined for the relative expression levels of *ABCB4*. Unpaired *t*-test was applied to test for statistical differences between the groups, with  $*P < 0.05$ .

*Abcb4* mRNA expression in *Mdr2*<sup>+/-</sup> mice, resulting in similar expression levels of *Abcb4* in *Mdr2*<sup>+/-</sup> and wt mice following viral challenge. We speculate that the processes driving upregulation of pro-inflammatory gene expression and recruitment of effector lymphocytes to the liver begin early after viral challenge and are linked to the specific metabolic profiles observed in noninfected mice rather than to those developing after viral infection. The absence of viral replication at day 8 p RRV in both *Mdr2*<sup>+/-</sup> and wt mice suggests that hepatic *Mdr2* reduction does not worsen the EHBA phenotype via promoting virus replication and direct virus cytopathic effects.

In validation studies using human tissue, we identified one African subject with a dual phenotype of EHBA and MDR3 disease harboring two nonsynonymous variants in *ABCB4*. In addition, the expression of *ABCB4* mRNA was decreased in livers from patients with EHBA and there was upregulation of pro-inflammatory genes compared with those of a fibrosing molecular phenotype. Comparison of liver transcriptomic data from studies in experimental RRV-induced EHBA with those in infants with EHBA is difficult given the plethora of environmental triggers implicated in the pathogenesis of human EHBA, including toxins and various viruses. Nevertheless, it is intriguing that *SELE*, encoding the endothelial vascular adhesion protein E-selectin, is upregulated in RRV-infected *Mdr2*<sup>+/-</sup> compared with wt mice, and is also found

to be preferentially expressed in infants with inflammatory EHBA and reduced *ABCB4* expression. Collectively, our data indicate that decreased hepatic expression of *ABCB4*, through either polymorphisms or inheritance of heterozygous deleterious mutations in this gene, may predispose infants to aggravated inflammatory responses in the liver, conferring susceptibility to the development of EHBA. This conclusion is further supported by a recent pilot study demonstrating that the prevalence of the heterozygous nonsynonymous variant p. A934T in *ABCB4* was higher in African-American subjects and segregated with worse outcome, as evidenced by the need for early transplantation in a cohort of 195 children with EHBA (unpublished data) (33). None of the 97 subjects who survived with the native liver beyond the first 4 years of life carried this variant.

Here we provide mechanistic data linking reduced PL transporter expression with the accumulation of biologically active lipid compounds (LPC) and polarization of immune responses, which if met by an environmental trigger may determine the degree of liver inflammation and disease phenotype. Whether in children with BA and pro-inflammatory phenotype, especially in those harboring nonsynonymous mutations in *ABCB4*, inflammatory PLs are retained and the PC/PE ratio is decreased requires further investigations. In addition, future studies may aim at better understanding the processes besides genetic predisposition



that reduce the expression of ABCB4/MDR3 in the neonatal liver, and at determining whether pharmacological interventions targeting MDR3 expression or activity, i.e., through fibrates (34), have the potential to ameliorate the disease phenotype of EHBA.

## METHODS

### Human Studies

**Case report.** The female patient was born small for gestational age at a Kenyan refugee camp (birth weight 1.5 kg), and was noted to be jaundiced at 7 months of age. She was diagnosed with PFIC3/MDR3 disease based on clinical genetic testing, which revealed two nonsynonymous variants in *ABCB4* (c.2363G>A [p.R788Q] and c.101C>T [p.T34M]), interpreted as pathogenic and as variant of uncertain significance, respectively. She presented to our center at 13 months of age with serum biochemistries notable for significant cholestasis (conjugated bilirubin 13 mg/dl, alkaline phosphatase 700 IU/l, gamma-glutamyltransferase 600 IU/l, total serum bile acids 128  $\mu$ mol/l), moderate hepatocellular injury (aspartate transaminase 400 IU/l and alanine transaminase 200 IU/l), and with coagulopathy (prothrombin time 19.5 s). The patient developed ascites, variceal bleeding, and ultimately underwent liver transplantation at 23 months of age. The explanted liver showed histomorphological features of MDR3 disease and EHBA.

**Hepatic microarray studies.** Relative *ABCB4* gene expression levels were analyzed in gene expression data originally obtained from hepatic microarray studies carried out on patients with EHBA at the time of diagnosis by intrahepatic cholangiograms (14). Detailed information on handling of liver biopsy samples, protocols for RNA labeling, chip hybridization and signals, internal controls, normalization procedures, and analysis of gene expression were deposited in Gene Expression Omnibus (GEO: GSE46995). The original study protocol conformed to the ethical guidelines of the 1975 Declaration of Helsinki and was approved by the human research committees of all participating institutions.

### Murine Studies

*Abcb4* (*Mdr2*)<sup>-/-</sup> mice were originally derived in the FVB strain (35) and then backcrossed into the BALB/c strain in the laboratory of Dr Lammert (Homburg/Germany) (4). In the established murine EHBA model, 1.5  $\times$  10<sup>6</sup> focus forming units (ffu) of rhesus rotavirus (RRV) is injected postnatally into BALB/c mice leading to bile duct obstruction (12). As a way to attenuate the EHBA phenotype, a lower dose of 0.5  $\times$  10<sup>6</sup> ffu of RRV was injected intraperitoneally at day of life 2. All mice were bred in-house and kept in conventional conditions. All protocols were approved by the Animal Care and Use Committee of the Cincinnati Children's Research Foundation.

### Phenotype of EHBA

The EHBA phenotype was assessed on day 8 p RRV challenge. Plasma total bilirubin concentration was measured using a colorimetric assay (Pierce Chemical, Rockford, IL). Zinc-fixed, paraffin-embedded extrahepatic bile ducts were sectioned and stained with hematoxylin and eosin, and patency was assessed on longitudinal sections by investigators blinded to the group assignment (A.N.C., A.G.M.), as previously performed in studies on experimental EHBA (31).

### iNOS Immunohistochemistry

Zinc-fixed mouse liver sections (5  $\mu$ m) were subjected to antigen retrieval consisting of heat at high pressure for 15 min in 1 M sodium citrate buffer, pH 6.0. Primary antibody against iNOS (rabbit; Abcam: Ab15323, Cambridge, UK) was diluted at a ratio of 1:100 with blocking solution and incubated at 4 °C overnight. Biotin-SP-conjugated Goat anti-rabbit (Jackson ImmunoResearch: 111-065-

003; West Grove, PA) was applied at 1:1,000 dilution and incubated for 2 h at room temperature.

### Protein Blot Analysis

Crude protein extracts from livers of neonatal mice were prepared by sonication on ice in RIPA Buffer. Lysates were centrifuged for 20 min at 14,000 rpm at 4 °C, and the supernatants were used for sodium dodecyl sulfate-polyacrylamide gel electrophoresis on a 4–12% acrylamide Bis-Tris gel (Invitrogen, Carlsbad, CA) followed by transfer to a nitrocellulose membrane. Immunoblotting was performed with anti-MDR3 antibody (Kamiya Biomedical, Tukwila, WA) or anti-actin antibody (Santa Cruz Biotechnology, Santa Cruz, CA) diluted a ratio of 1:1,000 in 2.5% bovine serum albumin blocking buffer followed by washes and incubation with a secondary antibody conjugated to horseradish peroxidase at 1:2,000 dilution. Blots were developed with Super Signal West Pico (Thermo Scientific, Florence, KY). The molecular weights of ABCB4-encoded membrane-bound P-glycoprotein and of actin are 140 and 43 kDa, respectively.

### Hepatic Mononuclear Cell Isolation, Flow Cytometric Analysis

Mice were killed and perfused with 10  $\mu$ g of collagenase through the portal vein. Hepatic mononuclear cells were isolated as previously reported by our group (36). Following red cell lysis and washes, single-cell suspensions were stained with PerCP-, PE-, APC-, and FITC- conjugated antibodies against CD3, CD8, NK, and CD4, respectively. Cell counts were acquired on an Accuri flow cytometer (BD Biosciences, Franklin Lakes, NJ). Flow cytometric data were compensated and analyzed using FlowJo Tree software (FlowJo LLC, Ashland, OR).

### Quantitative PCR

Multiplex qPCR using the TaqMan Mouse Immune Array (Applied Biosystems, Foster City, CA) with genes encoding 88 cytokines and chemokines and 8 housekeeping genes and candidate SYBR green qPCR were performed as reported by our group before (37).

### RNAseq

For RNAseq studies, total RNA was isolated from snap-frozen samples from lobe 2 of livers from 10-day-old mice born to *Mdr2*<sup>+/-</sup> parental mice, kept as littermates until the time of tissue harvest. RNAseq libraries were prepared with the Illumina TruSeq RNA preparation kit (Illumina, San Diego, CA) and sequenced on the Illumina Hi-Seq 2000, as previously described (38). Differentially expressed genes with a fold change  $\geq$  2.0 and  $p < 0.05$  between *Mdr2*<sup>+/-</sup> and *Mdr2*<sup>+/+</sup> neonatal mice were submitted to pathway enrichment analysis with ToppFun application from the ToppGene Suite, which uses unbiased methods to assess pathway enrichment (39). Raw and normalized data are accessible through NCBI's Gene Expression Omnibus (GEO accession number GSE78514).

### Global Lipidomic and Targeted Phospholipid Analysis by Liquid Chromatography–Mass Spectrometry

Liver tissue (lobe 1) was obtained from 10-day-old mice and subjected to exhaustive solvent extraction for lipids. Global lipidomics analysis was performed on a Xevo G2-S quadrupole time-of-flight mass spectrometer (MS) interfaced with an Acquity ultra-high-performance liquid chromatography (UPLC) system (Waters, Milford, MA) operated in electrospray ionization mode. An Acquity CSH C18 UPLC column was used to chromatographically separate components over 20 min gradient elution. Compounds were ionized with electrospray and positive and negative ions acquired over the mass range of 50–1,200 Da with high resolution. Deconvolution, peak alignment, and preliminary normalization were conducted on raw metabolomics data with Progenesis QI (Waters). Each compound ion feature was annotated by elution time with  $m/z$ . Raw data were normalized by total compound ion intensity and with a global scalar derived from logarithmic ratio of each sample to the

reference. Accurate molecular mass ( $m/z$ ) was used to search against HMDB and lipid MAPS database for putative identification.

**Targeted phosphatidylcholine and phosphatidylethanolamine analysis.** Quantitative analysis of PC and PE was carried out using a Waters API triple quadrupole mass spectrometer interfaced with an Acquity UPLC system and operated in electrospray ionization mode with negative ion acquisition. PLs were extracted from liver tissue by the Folch procedure and were quantified using the PC and PE standards with multiple reaction monitoring function. Total PC and PE were calculated based on the summation of 13 major PC species and 20 major PE species detected in plasma or liver.

**Statistical Analysis**

Statistical significance was determined by unpaired *t*- or Fisher exact tests with a significance set at  $P < 0.05$ . Multivariate analysis, i.e., principal component analysis for global lipidomics data, was conducted in R environment for statistical programming. Compound ions acquired from both positive and negative modes from the same sample were combined in the principal component analysis. Normalized abundance (area of feature peak normalized by the total compound ion abundance from that sample) of each compound ion was used in the analysis.

**ACKNOWLEDGMENTS**

We thank James Heubi (CCHMC) for the careful review of the manuscript and his thoughtful suggestions. We are grateful to Pranav Shivakumar for assistance in several of the experiments, and to Sujit Mohanty and Bryan Donnelly for providing primers and control cDNA for studies related to rotavirus replication.

**STATEMENT OF FINANCIAL SUPPORT**

The National Institute of Diabetes, Digestive and Kidney Diseases (NIDDK) grant DK095001 supported this study (to A.G.M.). The project was supported in part by PHS Grant P30 DK078392 (Pathology Core, Gene expression Core, Bioinformatics) of the Digestive Disease Research Core Center in Cincinnati, by the Childhood Liver Disease Research and Education Network (ChILDReN) Grant: 5U01DK062453-12, National Institutes of Health Level VI Fellowship Award (to A.N.C.), by the American Liver Foundation Postdoctoral Research Fellowship Award (to A.N.C.), by the 2013 American Association for the Study of Liver Diseases Fellow Research Award, by National Institutes of Health Training Grant 5T32DK007727-18 (to A.N.C.), and by the National Center for Research Resources, and the National Center for Advancing Translational Sciences, National Institutes of Health, through Grant 8 UL1 TR000077-04.

Disclosure: The authors disclose no conflict of interest.

**REFERENCES**

1. Davit-Spraul A, Gonzales E, Baussan C, Jacquemin E. The spectrum of liver diseases related to ABCB4 gene mutations: pathophysiology and clinical aspects. *Semin Liver Dis* 2010;30:134–46.
2. Poupon R, Arrive L, Rosmorduc O. The cholangiographic features of severe forms of ABCB4/MDR3 deficiency-associated cholangiopathy in adults. *Gastroenterol Clin Biol* 2010;34:380–7.
3. Vij M, Safwan M, Shanmugam NP, Rela M. Liver pathology in severe multidrug resistant 3 protein deficiency: a series of 10 pediatric cases. *Ann Diagn Pathol* 2015;19:277–82.
4. Lammert F, Wang DQ, Hillebrandt S, et al. Spontaneous cholecysto- and hepatolithiasis in *Mdr2*<sup>-/-</sup> mice: a model for low phospholipid-associated cholelithiasis. *Hepatology* 2004;39:117–28.
5. Gudbjartsson DF, Helgason H, Gudjonsson SA, et al. Large-scale whole-genome sequencing of the Icelandic population. *Nat Genet* 2015;47:435–44.
6. Dixon PH, Weerasekera N, Linton KJ, et al. Heterozygous MDR3 missense mutation associated with intrahepatic cholestasis of pregnancy: evidence for a defect in protein trafficking. *Hum Mol Genet* 2000;9:1209–17.

7. Ziolk M, Barbu V, Rosmorduc O, et al. ABCB4 heterozygous gene mutations associated with fibrosing cholestatic liver disease in adults. *Gastroenterology* 2008;135:131–41.
8. Degiorgio D, Crosignani A, Colombo C, et al. ABCB4 mutations in adult patients with cholestatic liver disease: impact and phenotypic expression. *J Gastroenterol* 2015;51:271–80.
9. Gordo-Gilart R, Hierro L, Andueza S, et al. Heterozygous ABCB4 mutations in children with cholestatic liver disease. *Liver Int* 2015;36:258–67.
10. Goldschmidt ML, Mourya R, Connor J, et al. Increased frequency of double and triple heterozygous gene variants in children with intrahepatic cholestasis. *Hepatol Res* 2015;46:306–11.
11. Li Z, Agellon LB, Allen TM, et al. The ratio of phosphatidylcholine to phosphatidylethanolamine influences membrane integrity and steatohepatitis. *Cell Metab* 2006;3:321–31.
12. Shivakumar PCK, Sabla GE, Miethke A, et al. Obstruction of extrahepatic bile ducts by lymphocytes is regulated by IFN-gamma in experimental biliary atresia. *J Clin Invest*. 2004;114:322–9.
13. Li J, Besho K, Shivakumar P, et al. Th2 signals induce epithelial injury in mice and are compatible with the biliary atresia phenotype. *J Clin Invest* 2011;121:4244–56.
14. Besho K, Mourya R, Shivakumar P, et al. Gene expression signature for biliary atresia and a role for interleukin-8 in pathogenesis of experimental disease. *Hepatology* 2014;60:211–23.
15. Moyer K, Kaimal V, Pacheco C, et al. Staging of biliary atresia at diagnosis by molecular profiling of the liver. *Genome Med* 2010;2:33.
16. Moustafa T, Fickert P, Magnes C, et al. Alterations in lipid metabolism mediate inflammation, fibrosis, and proliferation in a mouse model of chronic cholestatic liver injury. *Gastroenterology* 2012;142:e112.
17. Hardikar W, Ananthanarayanan M, Suchy FJ. Differential ontogenic regulation of basolateral and canalicular bile acid transport proteins in rat liver. *J Biol Chem* 1995;270:20841–6.
18. Cui YJ, Cheng X, Weaver YM, et al. Tissue distribution, gender-divergent expression, ontogeny, and chemical induction of multidrug resistance transporter genes (*Mdr1a*, *Mdr1b*, *Mdr2*) in mice. *Drug Metab Dispos* 2009;37:203–10.
19. Li ZZ, Berk M, McIntyre TM, et al. Hepatic lipid partitioning and liver damage in nonalcoholic fatty liver disease: role of stearyl-CoA desaturase. *J Biol Chem* 2009;284:5637–44.
20. Devaux PF. Static and dynamic lipid asymmetry in cell membranes. *Biochemistry* 1991;30:1163–73.
21. Walkey CJ, Yu L, Agellon LB, et al. Biochemical and evolutionary significance of phospholipid methylation. *J Biol Chem* 1998;273:27043–6.
22. Ling J, Chaba T, Zhu LF, Jacobs RL, Vance DE. Hepatic ratio of phosphatidylcholine to phosphatidylethanolamine predicts survival after partial hepatectomy in mice. *Hepatology* 2012;55:1094–102.
23. Ikenaga N, Liu SB, Sverdlow DY, et al. A new *Mdr2*(<sup>-/-</sup>) mouse model of sclerosing cholangitis with rapid fibrosis progression, early-onset portal hypertension, and liver cancer. *Am J Pathol* 2015;185:325–34.
24. Sontag TJ, Chellan B, Getz GS, Reardon CA. Differing rates of cholesterol absorption among inbred mouse strains yield differing levels of HDL-cholesterol. *J Lipid Res* 2013;54:2515–24.
25. Trivedi PJ, Weston CJ, Webb GJ, et al. Serum alkaline phosphatase in multidrug resistance 2 (*Mdr2*(<sup>-/-</sup>)) knockout mice is strain specific. *Hepatology* 2016;63:346.
26. Krones E, Erwa W, Trauner M, Fickert P. Serum alkaline phosphatase levels accurately reflect cholestasis in mice. *Hepatology* 2015;62:981–3.
27. Yan JJ, Jung JS, Lee JE, et al. Therapeutic effects of lysophosphatidylcholine in experimental sepsis. *Nat Med* 2004;10:161–7.
28. Sakata-Kaneko S, Wakatsuki Y, Usui T, et al. Lysophosphatidylcholine upregulates CD40 ligand expression in newly activated human CD4+ T cells. *FEBS Lett* 1998;433:161–5.
29. Coutant F, Perrin-Cocon L, Agaoglu S, et al. Mature dendritic cell generation promoted by lysophosphatidylcholine. *J Immunol* 2002;169:1688–95.

30. Asai A, Miethke A, Bezerra JA. Pathogenesis of biliary atresia: defining biology to understand clinical phenotypes. *Nat Rev Gastroenterol Hepatol* 2015;12:342–52.
31. Shivakumar P, Sabla GE, Whittington P, et al. Neonatal NK cells target the mouse duct epithelium via Nkg2d and drive tissue-specific injury in experimental biliary atresia. *J Clin Invest* 2009;119:2281–90.
32. Shivakumar P, Sabla G, Mohanty S, et al. Effector role of neonatal hepatic CD8+ lymphocytes in epithelial injury and autoimmunity in experimental biliary atresia. *Gastroenterology* 2007;133:268–77.
33. Mezina A, Gandhi K, Sabo A, et al. Abstract: whole exome sequencing identifies *ABCB4* gene variants as modifiers of biliary atresia outcomes. *Gastroenterology* 2014;146:S-928.
34. Chianale J, Vollrath V, Wielandt AM, et al. Fibrates induce *mdr2* gene expression and biliary phospholipid secretion in the mouse. *Biochem J* 1996;314 (Pt 3): 781–6.
35. Smit JJ, Schinkel AH, Oude Elferink RP, et al. Homozygous disruption of the murine *mdr2* P-glycoprotein gene leads to a complete absence of phospholipid from bile and to liver disease. *Cell* 1993;75:451–62.
36. Lages CS, Simmons J, Choungnet CA, et al. Regulatory T cells control the CD8 adaptive immune response at the time of ductal obstruction in experimental biliary atresia. *Hepatology* 2012;56:219–27.
37. Lages CS, Simmons J, Maddox A, et al. The dendritic cell-T helper 17-macrophage axis controls cholangiocyte injury and disease progression in murine and human biliary atresia. *Hepatology* 2017;65:174–88.
38. Miethke AG, Zhang W, Simmons J, et al. Pharmacological inhibition of apical sodium-dependent bile acid transporter changes bile composition and blocks progression of sclerosing cholangitis in multidrug resistance 2 knockout mice. *Hepatology* 2016;63:512–23.
39. Chen J, Bardes EE, Aronow BJ, et al. ToppGene Suite for gene list enrichment analysis and candidate gene prioritization. *Nucleic Acids Res* 2009;37:W305–11.